# Time-Domain Iterative Multiregion Technique for 3-D Scattering and Radiation Problems

Fatih Kaburcuk, Veysel Demir, *Member, IEEE*, Atef Z. Elsherbeni, *Fellow, IEEE*, Ercument Arvas, *Fellow, IEEE*, and Joseph R. Mautz, *Life Fellow, IEEE*

*Abstract*—Integration of the finite-difference time-domain (FDTD) method into the iterative multiregion (IMR) technique, an iterative approach used to solve large-scale electromagnetic scattering and radiation problems, is presented in this paper. The idea of the IMR technique is to divide a large problem domain into smaller subregions, solve each subregion separately, and combine the solutions of subregions after introducing the effect of interaction to obtain solutions at multiple frequencies for the large domain. Solutions of the subregions using frequency domain solvers has been the preferred approach as such; solutions using time domain solvers require computationally expensive bookkeeping of time signals. In this paper, we present an algorithm that makes it feasible to use the FDTD method, a time domain numerical technique, in the IMR technique to obtain solutions at a prespecified number of frequencies in a single simulation. A hybrid method integrated into the IMR technique is also presented in this paper. This hybrid method combines the desirable features of the FDTD method and the method of moments (MoM) to solve radiation problems more efficiently. As a result, a considerable reduction in memory storage requirements and computation time is achieved.

*Index Terms*—Electromagnetic scattering, finite-difference time-domain (FDTD) methods, hybrid solution methods, iterative methods, moment methods.

## I. INTRODUCTION

S OLUTION of large-scale electromagnetic scattering and radiation problems has been one of the major challenges of computational electromagnetics because the solution of such problems requires long computation time and large computer memory. In this paper, we present an algorithm that allows us to use the finite-difference time-domain (FDTD) method in the iterative multiregion (IMR) technique, a divide and conquer algorithm, to obtain solutions at a prespecified number of frequencies.

The decomposition of a problem domain into smaller domains is known as the domain decomposition method (DDM) [1]–[17], which in general requires either common boundaries or overlapping regions between subregions. It is possible to solve each subregion with the same method such as finite-element method (FEM) [3]–[7] or finite-difference frequency-domain (FDFD) method [8]–[13]. IMR is one of such methods that divides a problem space into smaller subregions. In the case of IMR, a problem space contains multiple objects with separations from each other, and each subregion contains one or more of the objects. The subregions do not need to have common boundaries or overlapping regions.

IMR, as originally introduced by Al Sharkawy *et al.* [9]–[12], uses the FDFD method to solve Maxwell's equations in subregions to calculate the scattering from many objects. This technique requires the solution of the fields in the subregions a number of times instead of one solution of the complete computational domain at a single frequency. In this paper, we adapt the use of the FDTD method instead of the FDFD method; as a consequence, a problem can be solved at a number of frequencies instead of a single frequency in a single simulation. In the IMR technique, scattered fields (SFs) confined to each subregion are calculated in the time domain, but radiation from one subregion to another is calculated in the frequency domain; thus, time domain to frequency domain and frequency domain to time domain transformations are needed. A key point in this paper is the time waveform construction (TWC) used to obtain the frequency domain to time domain transformations; we present an algorithm to construct time-limited waveforms whose frequency spectrums contain the required magnitudes and phases of the prespecified frequencies.

The iterative procedure in [9]–[12] is similar to the procedure denoted as the iterative field bouncing (IFB) method and described briefly in [14]. The DDM using the FDTD method [15] and using the fast multipole method [16] was used to solve a two-dimensional sparse multicylinder scattering problem. The multiple-region FDTD (MR/FDTD) proposed in [17] was introduced to solve a sparse modeling problem. In [15]–[17], the interaction and coupling effects between the objects are not considered very much because the separation distances between the objects are much larger than the largest dimension of one object.

### A. IMR Technique Using FDTD Method

In this paper, the FDTD method is integrated into the IMR technique to obtain solutions at multiple frequencies in a single IMR simulation using broadband excitation waveforms. The

procedure of the presented technique is used to analyze large-scale radiation and scattering problems which are difficult to handle using the conventional FDTD method.

In the case of scattering problems, a large-scale scattering problem is divided into smaller separated subregions, and each subregion is solved using the FDTD method independently. In each subregion, the SFs are calculated due to the same original incident plane wave. Then, electric and magnetic surface currents are calculated from the SFs over an imaginary surface (IS) of each subregion, using the surface equivalence principle [18] in frequency domain at a finite number of frequencies. Radiated fields generated by these currents are imposed as the new excitation fields on the opposing subregions in a new iteration. Since the new excitation fields are in the frequency domain at a number of frequencies, these fields must be converted into time-limited waveforms, using a TWC algorithm which obtains the magnitudes and phases of the desired frequencies, before exciting the FDTD problem space.

In the case of radiation problems, one of the subregions contains an antenna, and other subregions contain scattering objects. First, the antenna is driven in isolation so that there is no incident field in the subregion containing the driven antenna, and the incident fields in all the other subregions consist of the field of the driven antenna in isolation.

### B. IMR Technique Using Hybrid Method

Moreover, a hybrid method which combines the desirable features of the method of moments (MoM) and the FDTD method is also integrated into the IMR technique in this paper. Such a hybrid method has been extensively studied in [19]–[22] to simulate the interaction between a linear antenna and a scattering object. In [19] and [20], the coupling between subregions is simulated by employing the equivalence principle on the boundary surface surrounding each subregion. In [21] and [22], the electromagnetic coupling is performed between the scattering objects by applying the equivalence principle and the current distribution on the surface of an antenna. Their iterative approach of a hybrid method provides the solution at a single frequency in a single simulation. In this work, however, we integrate the FDTD method and MoM into the IMR technique to obtain solutions at multiple frequencies using the TWC algorithm in a single IMR simulation.

### C. Speeding Up Techniques

Initially, the SF formulation [23] has been used to excite the FDTD domains. The SF formulation requires the computation of new excitation fields at all field points in the problem space. It has been realized that a considerable amount of computation time is spent for the calculation of new excitation fields due to the fictitious surface currents. Therefore, the total-field SF (TF/SF) technique [24] is used to speed up the calculation of the new excitation fields. Thus, these fields are calculated on the TF/SF boundary rather than the entire computational domain in subregions. Then, an interpolation process is applied to source points over the IS and observation points on the TF/SF
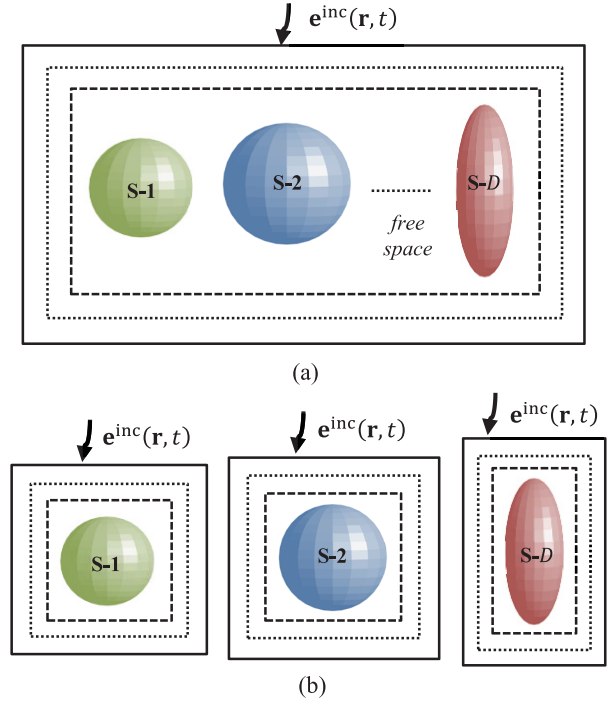


Fig. 1. Scattering from multiple objects: (a) original problem and (b) unconnected subregions. (Dashed line: TF/SF boundary, dotted line: IS, and solid line: CPML outer boundary).

boundary in subregions. These two techniques provide remarkable reduction in the computation time of the new excitation fields.

## II. IMR TECHNIQUE FOR THE SCATTERING PROBLEMS

### A. Objective

The objective for the scattering problem is to determine the bistatic radar cross sections (RCSs) at multiple angular frequencies $\{\omega = \omega_n, n = 1, 2, \ldots, N\}$ of a group of scattering objects. Here, $\omega_n$ is one of $N$ known angular frequencies of interest. Illustrated in Fig. 1, the problem space is divided into $D$ unconnected subregions. For simplicity, there is one scattering object in each subregion. The subregion boundaries are terminated by convolution perfectly matched layers (CPMLs) [25] indicated by solid lines in Fig. 1 to simulate open-space scattering problems.

The group of scattering objects is illuminated by a plane wave. For $\{d = 1, 2, \ldots, D\}$, the electromagnetic field of this plane wave on the TF/SF boundary in subregion $d$ consists of the electric field $\mathbf{e}^{\text{inc}}(\mathbf{r}, t)$ and the magnetic field $\mathbf{h}^{\text{inc}}(\mathbf{r}, t)$ given by

$$\mathbf{e}^{\text{inc}}(\mathbf{r}, t) = \mathbf{E}_0^{\text{inc}} g\left(t - t_0 - \left(\hat{\mathbf{k}} \cdot (\mathbf{r} - \mathbf{r}_0)\right)/c\right) \tag{1}$$

$$\mathbf{h}^{\text{inc}}(\mathbf{r}, t) = \frac{1}{\eta}\left(\hat{\mathbf{k}} \times \mathbf{E}_0^{\text{inc}}\right) g\left(t - t_0 - \left(\hat{\mathbf{k}} \cdot (\mathbf{r} - \mathbf{r}_0)\right)/c\right), \tag{2}$$

where $\hat{\mathbf{k}}$ is the unit vector that is constant and is in the direction of propagation of the incident plane wave, $\mathbf{E}_0^{\text{inc}}$ is a purely real vector that is perpendicular to $\hat{\mathbf{k}}$, $\mathbf{r}$ is the radius vector from the

global origin which is somewhere in the vicinity of the scattering objects, $c$ is the speed of light, $t$ is time, $\mathbf{r}_0$ is a spatial shift, $t_0$ is a time shift, and $\eta$ is the intrinsic impedance of the medium. If $\mathbf{e}^{\text{inc}}$ is a combination of both orthogonal polarizations, then application of nonzero phase factors in each $\mathbf{E}_0^{\text{inc}}$ can be delayed until a solution is done for each polarization. The TF/SF boundary is shown in Fig. 1. The TF exists in the region between the scattering object in subregion $d$ and the TF/SF boundary in subregion $d$, and the SF exists beyond the TF/SF boundary in subregion $d$. The function $g(t)$ in (1) and (2) and its Fourier transform $G(\omega)$ are given by

$$g(t) = e^{-(t/\tau)^2} \tag{3}$$

$$G(\omega) = \tau\sqrt{\pi}e^{-(\tau\omega/2)^2}. \tag{4}$$

The bistatic RCS at $\omega_n$ is $\sigma_n$ given by

$$\sigma_n = \frac{4\pi r^2 |E_n^{\text{scat}}|^2}{|E_n^{\text{inc}}|^2}. \tag{5}$$

In (5), $E_n^{\text{scat}}$ is evaluated at the distance $r$ from the global origin, and $r$ is in the far field region of all the scattering objects.

### B. Iterative Procedure

The SF is the sum of the SFs found in the iterations. The iterations consist of iteration #$k$ for $\{k = 0, 1, 2, \ldots, K\}$. Iteration #0 is the initialization. The SF found in the initialization is the SF that would exist if the TF/SF boundary in each subregion, isolated from the other subregions, was illuminated by the incident electromagnetic field that consists of $\sum\limits_{n=1}^{N}$ of the $e^{j\omega_n t}$ dependent electric and magnetic fields whose coefficients of $e^{j\omega_n t}$ are the Fourier transforms at $\omega = \omega_n$ of the incident electric and magnetic fields (1) and (2). By the equivalent principle, electric and magnetic currents on the IS in the subregion radiate their part of the scattered electromagnetic field beyond the IS in the subregion and no field elsewhere, where elsewhere is the region bounded by the IS in the subregion. These electric and magnetic currents are due to the incident field on the TF/SF boundary. For $\{k = 1, 2, \ldots, K\}$, the SF found in the iteration #$k$ is the field of the electric and magnetic currents induced by the electric and magnetic currents found in iteration #$(k-1)$. For $\{d = 1, 2, \ldots, D\}\}$, the induced electric and magnetic currents on the IS in subregion $d$ radiate the part of the SF due to the illumination of the TF/SF boundary in subregion $d$ by the field of all the electric and magnetic currents of iteration #$(k-1)$ except those currents in subregion $d$. The iterative procedure is shown in Fig. 2.

*1) Initialization:* In the initialization, the set of operations to be described is done for $\{d = 1, 2, \ldots, D\}$. The TF/SF boundary in subregion $d$, isolated from all the other subregions, is illuminated by the incident electromagnetic field whose electric and magnetic fields are given by (1) and (2) whose Fourier transforms $\mathbf{E}^{\text{inc}}(\mathbf{r}, \omega)$ and $\mathbf{H}^{\text{inc}}(\mathbf{r}, \omega)$ are given by

$$\mathbf{E}^{\text{inc}}(\mathbf{r}, \omega) = \mathbf{E}_0^{\text{inc}}G(\omega)e^{-j\omega(t_0 + (\hat{\mathbf{k}}\cdot(\mathbf{r}-\mathbf{r}_0))/c)} \tag{6}$$

$$\mathbf{H}^{\text{inc}}(\mathbf{r}, \omega) = \frac{1}{\eta}\left(\hat{\mathbf{k}} \times \mathbf{E}_0^{\text{inc}}\right)G(\omega)e^{-j\omega(t_0 + (\hat{\mathbf{k}}\cdot(\mathbf{r}-\mathbf{r}_0))/c)}, \tag{7}$$
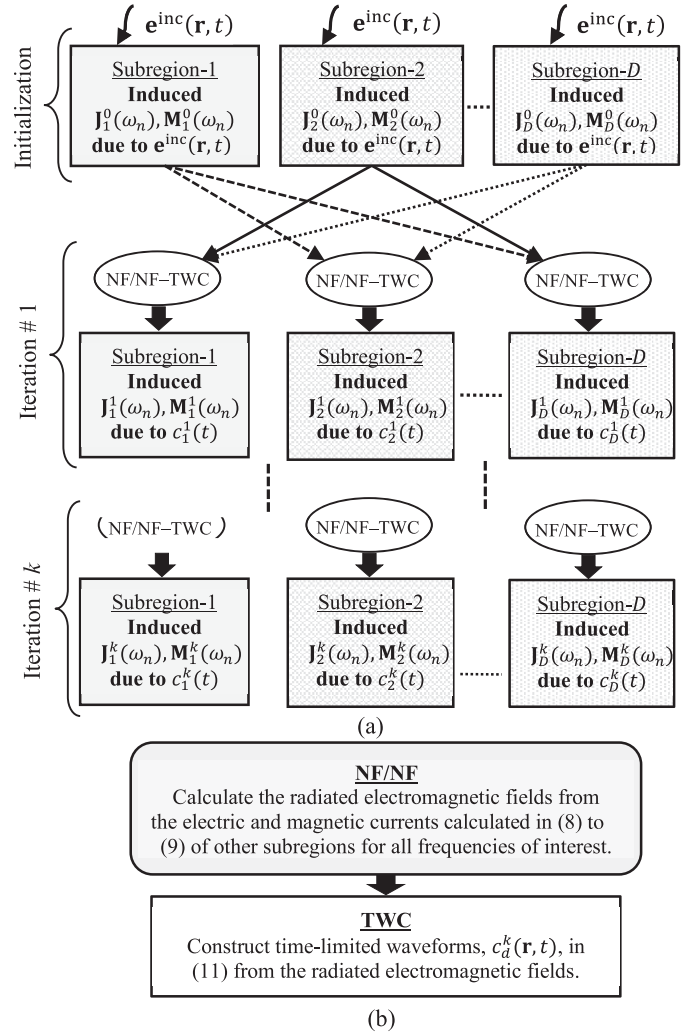


Fig. 2. (a) Iterative procedure between subregions. (b) NF/NF–TWC algorithm. (NF/NF, near field to near field; TWC, time waveform construction).

where $G(\omega)$ is given by (4). Henceforth, as in (6) and (1), a Fourier transform will be an upper case letter and its inverse will be the corresponding lower case letter. The TF/SF boundary in subregion $d$ and the IS in subregion $d$ are divided into subsurfaces. The vector $\mathbf{r}$ in (1) and (2) is sampled on each subsurface of the TF/SF boundary and a vector called $\mathbf{r}_{\text{IS}}$ is sampled on each subsurface of the IS. For each sample of $\mathbf{r}$, there are six rectangular components of the incident electromagnetic field: three rectangular components $\mathbf{e}^{\text{inc}}(\mathbf{r}, t)$ and three rectangular components of $\mathbf{h}^{\text{inc}}(\mathbf{r}, t)$. These six rectangular components of the incident field on the TF/SF boundary in subregion $d$ start an FDTD procedure that finds the six rectangular components of the scattered electromagnetic field $(\mathbf{e}_d^0(\mathbf{r}_{\text{IS}}, t), \mathbf{h}_d^0(\mathbf{r}_{\text{IS}}, t))$ at $\mathbf{r}_{\text{IS}}$ on the IS in subregion $d$. In $\mathbf{e}_d^0$ and $\mathbf{h}_d^0$, the superscript zero indicates the initialization, and the subscript $d$ indicates subregion $d$. Electric and magnetic currents $\mathbf{j}_d^0(\mathbf{r}_{\text{IS}}, t) = \hat{\mathbf{n}} \times \mathbf{h}_d^0(\mathbf{r}_{\text{IS}}, t)$ and $\mathbf{m}_d^0(\mathbf{r}_{\text{IS}}, t) = -\hat{\mathbf{n}} \times \mathbf{e}_d^0(\mathbf{r}_{\text{IS}}, t)$ and their Fourier transforms $\mathbf{J}_d^0(\mathbf{r}_{\text{IS}}, \omega) = \hat{\mathbf{n}} \times \mathbf{H}_d^0(\mathbf{r}_{\text{IS}}, \omega)$ and $\mathbf{M}_d^0(\mathbf{r}_{\text{IS}}, \omega) = -\hat{\mathbf{n}} \times \mathbf{E}_d^0(\mathbf{r}_{\text{IS}}, \omega)$ are defined at $\mathbf{r}_{\text{IS}}$ on the IS in subregion $d$ where $\hat{\mathbf{n}}$ is the outward directed unit vector that is perpendicular to the IS in subregion $d$.

For each combination of a sample of $\mathbf{r}$ and a sample of $\mathbf{r}_{\text{IS}}$, the Fourier transforms $\mathbf{J}_d^0(\mathbf{r}_{\text{IS}}, \omega)$ and $\mathbf{M}_d^0(\mathbf{r}_{\text{IS}}, \omega)$ are due to the Fourier transforms $\mathbf{E}^{\text{inc}}(\mathbf{r}, \omega)$ and $\mathbf{H}^{\text{inc}}(\mathbf{r}, \omega)$. Multiplication of $\mathbf{E}^{\text{inc}}(\mathbf{r}, \omega)$ and $\mathbf{H}^{\text{inc}}(\mathbf{r}, \omega)$ by $2\pi\delta(\omega - \omega_n)$ is accompanied by multiplication of $\mathbf{J}_d^0(\mathbf{r}_{\text{IS}}, \omega)$ and $\mathbf{M}_d^0(\mathbf{r}_{\text{IS}}, \omega)$ by $2\pi\delta(\omega - \omega_n)$, where $\delta$ is the Dirac delta function and $(1 \leq n \leq N)$. Now, the Fourier transforms $\mathbf{J}_d^0(\mathbf{r}_{\text{IS}}, \omega_n)$ $2\pi\delta(\omega - \omega_n)$ and $\mathbf{M}_d^0(\mathbf{r}_{\text{IS}}, \omega_n)$ $2\pi\delta(\omega - \omega_n)$ are due to the Fourier transforms $\mathbf{E}^{\text{inc}}(\mathbf{r}, \omega_n)\, 2\pi\delta(\omega - \omega_n)$ and $\mathbf{H}^{\text{inc}}(\mathbf{r}, \omega_n)\, 2\pi\delta(\omega - \omega_n)$. Taking inverse transforms and knowing that the inverse transform of $2\pi\delta(\omega - \omega_n)$ is $e^{j\omega_n t}$, we see that $\mathbf{J}_d^0(\mathbf{r}_{\text{IS}}, \omega_n)\, e^{j\omega_n t}$ and $\mathbf{M}_d^0(\mathbf{r}_{\text{IS}}, \omega_n)\, e^{j\omega_n t}$ are due to $\mathbf{E}^{\text{inc}}(\mathbf{r}, \omega_n)\, e^{j\omega_n t}$ and $\mathbf{H}^{\text{inc}}(\mathbf{r}, \omega_n)\, e^{j\omega_n t}$. Thus, a relation among Fourier transforms of time limited functions is converted to a relation among $e^{j\omega_n t}$ dependent time functions. The conversion is implemented by the setting $\omega = \omega_n$ in the Fourier transforms of the time limited functions and then multiplying them by $e^{j\omega_n t}$.

To do the conversion described in the previous paragraph where Fourier transforms of time limited responses due to Fourier transforms of time limited excitations are converted to $e^{j\omega_n t}$ dependent responses due to $e^{j\omega_n t}$ dependent excitations, we need to know the Fourier transforms $\mathbf{E}^{\text{inc}}(\mathbf{r}, \omega_n)$, $\mathbf{H}^{\text{inc}}(\mathbf{r}, \omega_n)$, $\mathbf{J}_d^0(\mathbf{r}_{\text{IS}}, \omega_n)$ and $\mathbf{M}_d^0(\mathbf{r}_{\text{IS}}, \omega_n)$. The Fourier transforms $\mathbf{E}^{\text{inc}}(\mathbf{r}, \omega_n)$ and $\mathbf{H}^{\text{inc}}(\mathbf{r}, \omega_n)$ are obtained by setting $\omega = \omega_n$ in (6) and (7). Also, $\mathbf{J}_d^0(\mathbf{r}_{\text{IS}}, \omega_n)$ and $M_d^0(\mathbf{r}_{\text{IS}}, \omega_n)$ are calculated concurrently with $\mathbf{j}_d^0(\mathbf{r}_{\text{IS}}, t)$ and $\mathbf{m}_d^0(\mathbf{r}_{\text{IS}}, t)$ by means of an on-the-fly numerical Fourier transform (NFT) [23] by which

$$\mathbf{J}_d^0(\mathbf{r}_{\text{IS}}, \omega_n) = \Delta t \sum_{i=1}^{N_{steps}} \mathbf{j}_{d,i}^0 e^{-j\omega_n i \Delta t} \tag{8}$$

$$\mathbf{M}_d^0(\mathbf{r}_{\text{IS}}, \omega_n) = \Delta t \sum_{i=1}^{N_{steps}} \mathbf{m}_{d,i}^0 e^{-j\omega_n i \Delta t}, \tag{9}$$

where $\Delta t$ is the duration of a time step, $\mathbf{j}_{d,i}^0$ and $\mathbf{m}_{d,i}^0$ are $\mathbf{j}_d^0(\mathbf{r}_{\text{IS}}, t)$ and $\mathbf{m}_d^0(\mathbf{r}_{\text{IS}}, t)$ at the $i$th time step, and $N_{\text{steps}}$ is the number of time steps over which $\left|\mathbf{j}_{d,i}^0\right|$ and $\left|\mathbf{m}_{d,i}^0\right|$ are appreciable.

*2) Iteration #k for $k \geq 1$:* For $\{(n = 1, 2, \ldots, N), d' = 1, 2, \ldots, D\}$, the electric and magnetic currents $\mathbf{J}_{d'}^{k-1}(\mathbf{r}_{\text{IS}}, \omega_n)\, e^{j\omega_n t}$ and $\mathbf{M}_{d'}^{k-1}(\mathbf{r}_{\text{IS}}, \omega_n)\, e^{j\omega_n t}$ were obtained in iteration $\#(k-1)$. In iteration $\#k$ for $k \geq 1$, the set of operations to be described is done for $\{(n = 1, 2, \ldots, N), d = 1, 2, \ldots, D\}$ In iteration $\#k$, the field of all of the electric and magnetic currents that were obtained in iteration $\#(k-1)$ except those for which $d' = d$ is incident on the TF/SF boundary in subregion $d$. Calculated in the frequency domain by using several near field/near field (NF/NF) transformations [18], this field, which consists of $(e^{j\omega_n t}, n = 1, 2, \ldots, N)$ dependent fields, is the time unlimited incident field.

Heretofore, $e^{-j\omega_n t}$ was not involved and the real part was taken after all manipulations with $e^{j\omega_n t}$ were done. If the real part is taken now, then one of the six rectangular components of the time unlimited incident field at one of the sample points $\mathbf{r}$ is

$$\breve{c}(\mathbf{r}, t) = \frac{1}{2} \sum_{n=1}^{N} \left[ C_n(\mathbf{r})\, e^{j\omega_n t} + C_n^*(\mathbf{r})\, e^{-j\omega_n t} \right] \tag{10}$$

where $C_n(\mathbf{r})$ is a previously calculated complex number and the asterisk denotes the complex conjugate. The corresponding component of the time limited incident field at the same $\mathbf{r}$ is chosen to be

$$c(\mathbf{r}, t) = g(t) \sum_{m=1}^{N} (B_m(\mathbf{r}))_d^k \cos\left(\omega_m t + (\theta_m(\mathbf{r}))_d^k\right) \tag{11}$$

whose Fourier transform is

$$C(\mathbf{r}, \omega) = \frac{1}{2} \sum_{m=1}^{N} \left\{ (B_m(\mathbf{r}))_d^k \left( \begin{array}{c} G(\omega - \omega_m)\, e^{j(\theta_m(\mathbf{r}))_d^k} \\ +G(\omega + \omega_m)\, e^{-j(\theta_m(\mathbf{r}))_d^k} \end{array} \right) \right\} \tag{12}$$

where $\left\{ (B_m(\mathbf{r}))_d^k, (\theta_m(\mathbf{r}))_d^k, m = 1, 2, \ldots, N \right\}$ are $2N$ real unknowns that are determined by substituting $\left( C(\mathbf{r}, \omega_n) = \frac{1}{2} C_n(\mathbf{r}), n = 1, 2, \ldots, N \right)$ into the $N$ complex equations that are obtained by setting $(\omega = \omega_n, n = 1, 2, \ldots, N)$ in (12)

$$\frac{1}{2} C_n(\mathbf{r}) = \frac{1}{2} \sum_{m=1}^{N} \left\{ \begin{array}{c} (B_m(\mathbf{r}))_d^k G(\omega_n - \omega_m)\, e^{j(\theta_m(\mathbf{r}))_d^k} \\ + (B_m(\mathbf{r}))_d^k G(\omega_n + \omega_m)\, e^{-j(\theta_m(\mathbf{r}))_d^k} \end{array} \right\} \tag{13}$$

where $(n = 1, 2, \ldots, N)$ and $C_n(\mathbf{r})$ appears in (10). If (13) holds, then an auxiliary equation, which is (13) with $C_n(\mathbf{r})$ replaced by $C_n^*(\mathbf{r})$ and $\omega_n$ replaced by $-\omega_n$, also holds because replacement of $\omega_n$ by $-\omega_n$ replaces the right-hand side of (13) by its complex conjugate.

Proceeding as in the initialization, we find the Fourier transforms of the electric and magnetic currents due to the Fourier transform (12). According to the conversion in the initialization, each of these Fourier transforms is evaluated at $\omega = \omega_n$ and multiplied by $e^{j\omega t}$. In particular, the Fourier transform (12) converts to $\frac{1}{2} C_n(\mathbf{r}) e^{j\omega_n t}$ in (10). In the same conversion with $\omega$ replaced by $-\omega_n$, the Fourier transform (12) converts to $\frac{1}{2} C_n^*(\mathbf{r}) e^{-j\omega_n t}$ in (10). The algorithm that uses the time limited waveform (11) to obtain the electric and magnetic currents which are the real parts of $\mathbf{J}_d^k(\mathbf{r}_{\text{IS}}, \omega_n)\, e^{j\omega_n t}$ and $\mathbf{M}_d^k(\mathbf{r}_{\text{IS}}, \omega_n)\, e^{j\omega_n t}$ is called the TWC algorithm.

*3) Reckoning at Iteration $\#K$:* A convergence criterion for the coefficients of $e^{j\omega_n t}$ in the temporal expression for the electric current is $\varepsilon_k$ defined by

$$\varepsilon_k = \frac{\|\mathbf{J}_d^k(\mathbf{r}_{\text{IS}}, \omega_n)\|}{\|\sum_{i=0}^{k} \mathbf{J}_d^i(\mathbf{r}_{\text{IS}}, \omega_n)\|} \times 100\% \tag{14}$$

where "$\| \|$" indicates the Euclidean norm [26] of the enclosed vector. The convergence criterion for the magnetic current is similar to that for the electric current. The iterations stop at iteration $\#K$ where $K$ is the first value of $k$ for which the convergence criterion is small for both the electric and magnetic current for $\{d = 1, 2, \ldots, D\}$ and $\{n = 1, 2, \ldots, N\}$.
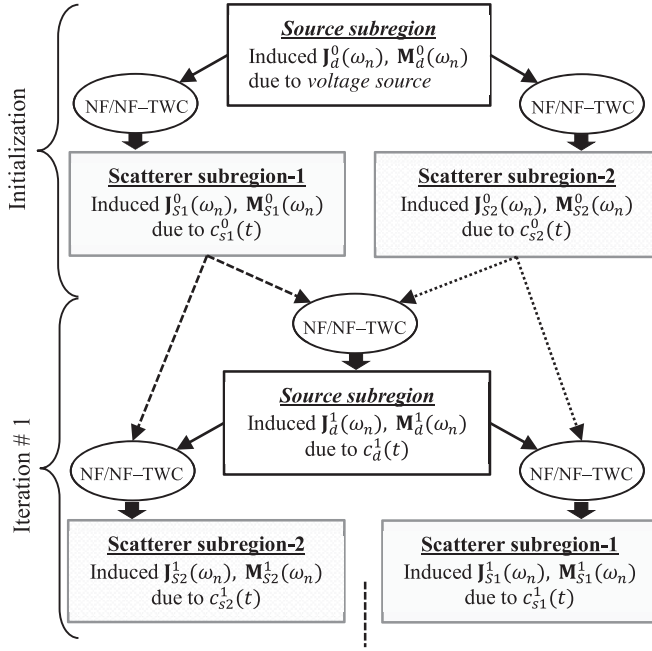
Fig. 3. Iterative procedure between source subregion and scatterer subregions.



Fig. 4. Geometry of the problem.



Fig. 5. Convergence ($\epsilon_k$) of the iteration steps.

After the initialization and iteration #$k$ for $\{k = 1, 2, \ldots, \}K$ are done, electric and magnetic currents $\mathbf{j}_d\left(\mathbf{r}_{\text{IS}}, t\right) = \mathrm{R} \sum_{k=0}^{K} \sum_{n=1}^{N} \mathbf{J}_d^k\left(\mathbf{r}_{\text{IS}}, \omega_n\right) e^{j\omega_n t}$ and $\mathbf{m}_d\left(\mathbf{r}_{\text{IS}}, t\right) = \mathrm{R} \sum_{k=0}^{K} \sum_{n=1}^{N} \mathbf{M}_d^k\left(\mathbf{r}_{\text{IS}}, \omega_n\right) e^{j\omega_n t}$ will be at $\mathbf{r}_{\text{IS}}$ on the IS in subregion $d$ for $\{d = 1, 2, \ldots, D\}$. The field scattered by all of the scatterers is the field radiated by all of the above electric and magnetic currents. Once evaluated in the far zone by using a near field to far field transformation [23], this SF can be used to obtain the phasor $E_n^{scat}$ that appears in (5).

## III. IMR TECHNIQUE FOR THE RADIATION PROBLEMS

In this section, we extend the iterative approach to radiation problems. The problem domain is divided into separate regions: one of them is the source subregion containing an antenna and the others are the scatterer subregions containing scattering objects. Illustrated in Fig. 3, the iterative procedure among the subregions of a radiation problem is similar to the iterative procedure for the scattering problem: the major difference is that the antenna is driven by a voltage source instead of an incident electric field.

In the initialization, the free-space field of the antenna is incident on the scatterer in each scatterer subregion, causing electric and magnetic currents to be induced on the IS in each scatterer subregion. These currents are the first bounce currents. In iteration #1, the induced currents that were obtained in the initialization on the IS in each scatterer subregion induce second bounce currents on the ISs in all the other scatterer subregions and the source subregion. The second bounce currents on the ISs in the scatterer subregions and the source subregion induce third bounce currents on the ISs. The arrows that point away from the upper box in iteration #1 shown in Fig. 3
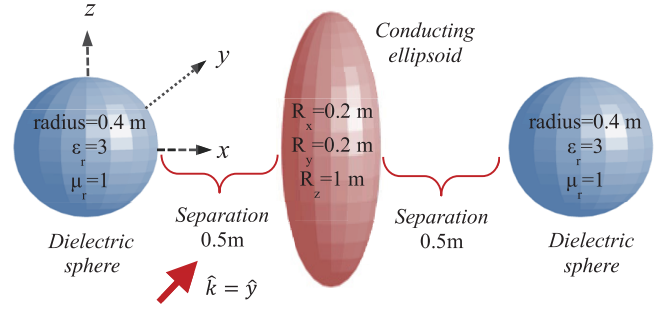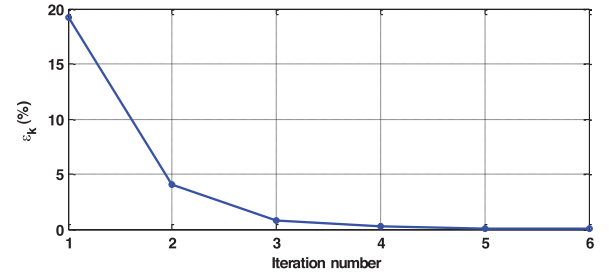
obtain the part of the third bounce currents that is induced by the second bounce currents on the IS in the source subregion. Thus, iteration #1 also obtains this part of the third bounce currents. Iteration #2 and subsequent iterations are repetitions of iteration #1.

## IV. NUMERICAL RESULTS

In this section, we test the performance of the proposed technique for solving 3-D scattering and radiation problems. The computer being used in this work has Intel Core i7-4770 CPU and 32 GB DDR RAM. The program is written and compiled in 64-bit MATLAB version 7.5.0.342 (R2007b).

Based on numerical experiments, $\varepsilon_k = 5\%$ in (14) is found sufficient to indicate that convergence is achieved since RCS values at desired frequencies do not change significantly for smaller values of $\varepsilon_k$.

### A. Results for Scattering Problem

A problem whose geometry is illustrated in Fig. 4 is analyzed to prove the validity of the IMR–FDTD technique. Two identical dielectric spheres with the relative permittivity of 3 and radius of 0.4 m and a conducting ellipsoid are placed along the $x$-axis with 0.5 m separation. The semiaxes of the conducting ellipsoid are 0.2, 0.2, and 1 m along the $x$-, $y$-, and $z$-axes, respectively. This problem space is excited by a plane wave that travels in the $y$-direction and has a $\theta$-polarized incident electric field. Both incident and scattered electric fields in (5) are $\theta$-polarized. The problem space is composed of cells with size 0.02 m in the $x$-, $y$-, and $z$-directions for the full domain simulation. As for the IMR simulation, a cell size 0.02 m is used in the ellipsoid subregion, whereas a cell size 0.04 m is used in the other subregions. It can be seen from Fig. 5 that the IMR
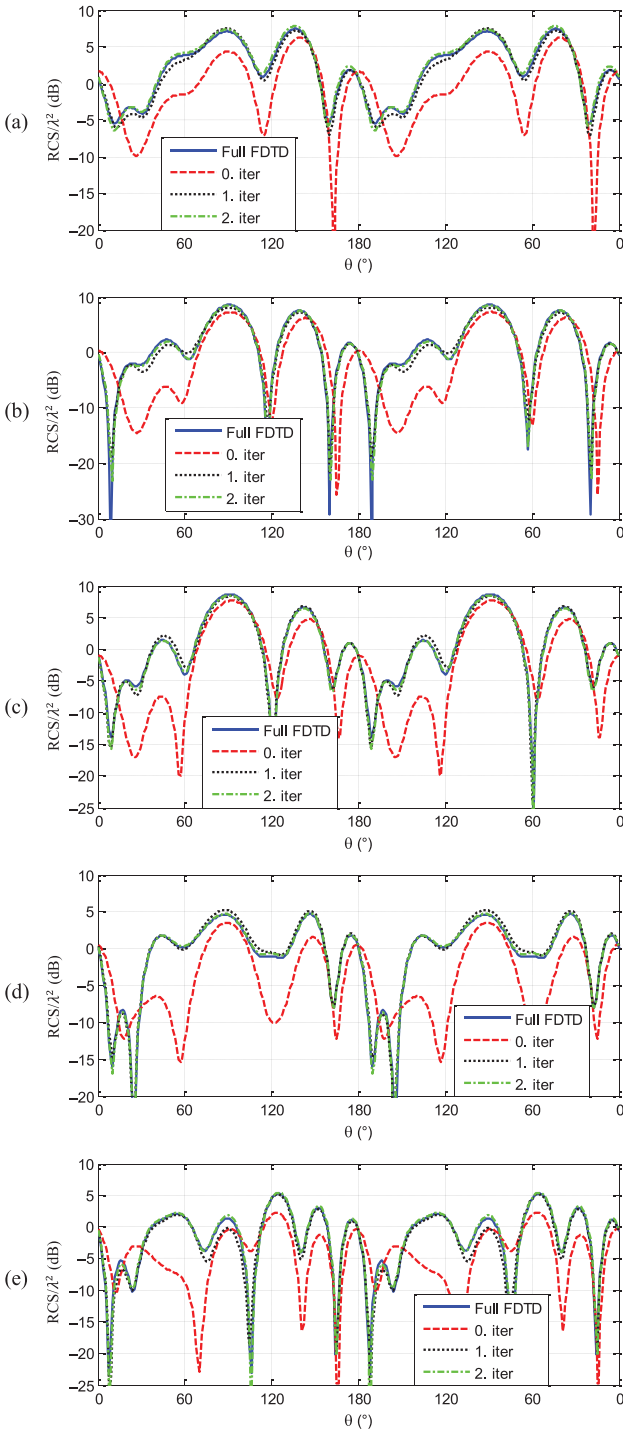
Fig. 6. Bistatic RCS/$\lambda^2$ for $xz$-plane cuts at frequencies: (a) 200, (b) 225, (c) 250, (d) 275, and (e) 300 MHz.



Fig. 7. Normalized average error for RCS in the $xz$-plane cut.



Fig. 8. Magnitude of the reflection coefficient of a single 0.5-m dipole antenna.

full domain and IMR technique results, the normalized average error for RCS in $xz$-plane cut is calculated using (15) and is shown in Fig. 7

$$\text{Error}(\omega_n) = \text{mean}\left(\frac{\left|\sigma^{\text{IMR}}(\omega_n) - \sigma^{\text{Full}}(\omega_n)\right|}{\max\left(\left|\sigma^{\text{Full}}(\omega_n)\right|\right)}\right) \times 100\% . \tag{15}$$

### B. Results for Radiation Problem

A radiation problem with a dipole antenna and scattering objects is analyzed to prove the validity of the IMR technique. In the problem, there is a 0.5-m dipole antenna configured as two rectangular rods with square base of side length equal to 31.25 mm. The thickness of the dipole is four cells in both $x$ and $y$ directions. A voltage source with 50-$\Omega$ internal impedance and 1-V magnitude is placed along four cells between the rods. A cell size of 7.8125 mm is used for the antenna. The antenna is simulated alone using the FDTD method to determine the frequency bands in which it radiates well. The frequencies 230, 240, 250, 260, and 270 MHz are found to be in the band of operation. Fig. 8 shows the magnitude of the reflection coefficient of the dipole antenna.

The geometry of the radiation problem is presented in Fig. 9, where the dipole antenna is placed a distance of 1.25 m away from two conductor shapes (shape-A and shape-B) along the $x$-direction. The separation between shapes is 2.5 m along the $x$-direction. The dimensions of the shape-A are 25 cm, 1 m, and 1 m along the $x$-, $y$-, and $z$-directions, respectively. The dimensions of shape-B on the $yz$-plane are shown in Fig. 9(b). The dimension of shape-B along the $x$-direction is 25 cm. The center of the dipole antenna is at the origin, the bases of the shapes A and B are at $z = -0.5$ m, and the leading edges of these bases are at $y = -0.5$ m and $-1.25$ m, respectively. A cell size

algorithm reaches the convergence criterion ($\epsilon_k \leq 5\%$). Fig. 6 shows the bistatic RCS/$\lambda^2$ for $xz$-plane cuts at 200, 225, 250, 275, and 300 MHz, where $\lambda$ is the free space wavelength. The data for other plane cuts are exactly over each other after two iterations with a 60% memory reduction in the storage requirements, but there is no significant change in the computation time. The computation time would be less and the memory reduction would be more for problems that have large separation between the objects. To prove the convergence of the
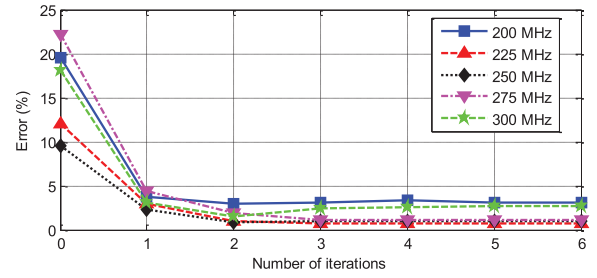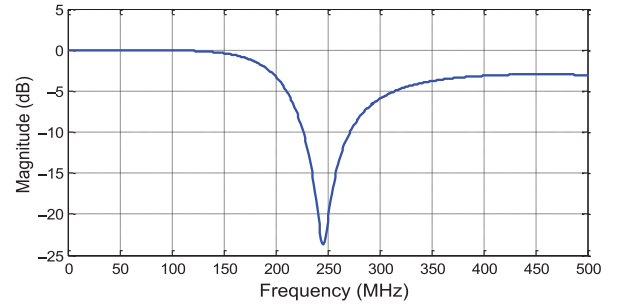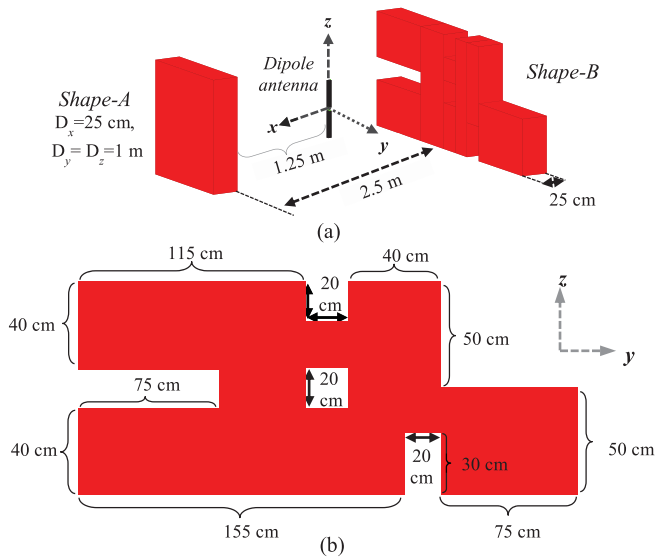
Fig. 9. (a) Geometry of the radiation problem and (b) geometry of the conductor shape-B on the *yz*-plane.
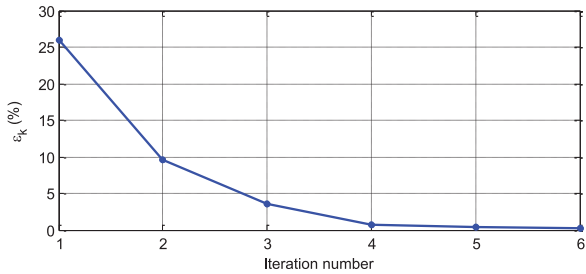


Fig. 10. Convergence ($\epsilon_k$) of the iteration steps.

of 15.625 mm on a side is used to simulate the scatterer subregions. It can be seen from Fig. 10 that the IMR algorithm reaches the convergence criterion ($\epsilon_k \leq 5\%$) after three iterations. Fig. 11 shows the power gain patterns (Gain$_\theta$) of the configuration for *xz*-plane cuts. The data for other plane cuts are exactly over each other after three iterations with a 93% memory reduction in the storage requirements. The computation time of the IMR technique is 45% less than that of the full domain after three iterations. To prove the convergence of the results of the IMR and the full domain solution, the normalized average error for Gain$_\theta$ in *xz*-plane cuts is calculated using (16) and shown in Fig. 12

$$\text{Error}\,(\omega_n) = \text{mean} \left( \frac{\left| \text{Gain}^{IMR}(\omega_n) - \text{Gain}^{Full}(\omega_n) \right|}{\max\left( \left| \text{Gain}^{Full}(\omega_n) \right| \right)} \right) \\ \times 100\%. \tag{16}$$

## V. IMR ALGORITHM AS A HYBRID METHOD

A problem domain shown in Fig. 13 is divided into two subregions: one is the MoM subregion containing a thin wire antenna and the other is the FDTD subregion containing a dielectric object. The iterative procedure between subregions is shown in Fig. 14. The procedure consists of the initialization and iteration #*k* for ($k = 1, 2, \ldots, K$). For $k \geq 2$, iteration #*k* is a repetition of iteration #1.
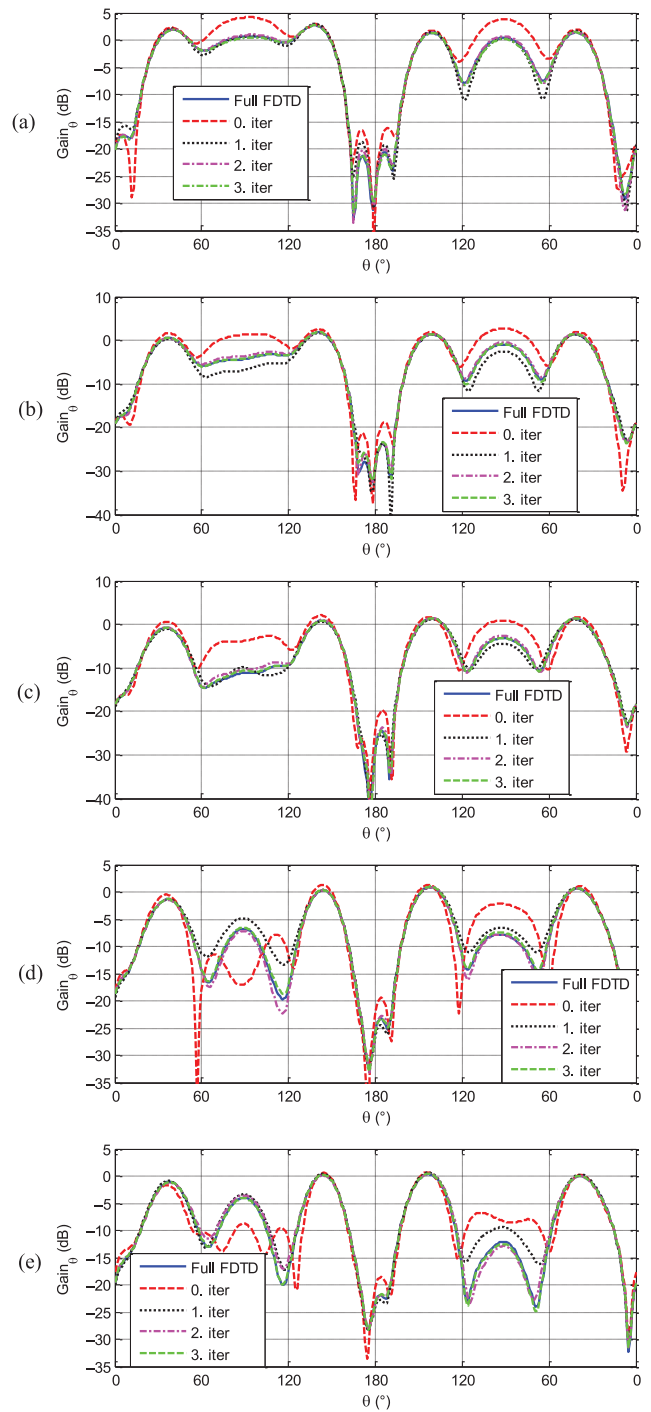


Fig. 11. Power gain pattern (Gain$_\theta$) for *xz*-plane cut at frequencies: (a) 230, (b) 240, (c) 250, (d) 260, and (e) 270 MHz.
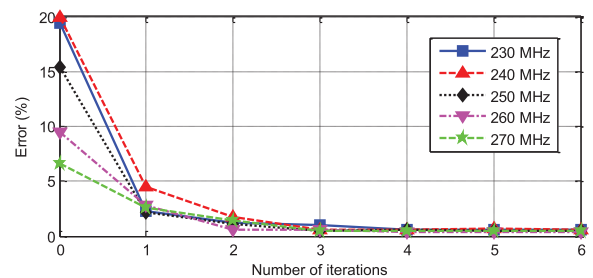


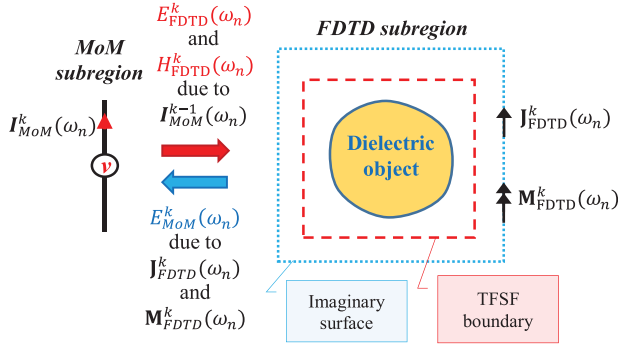Fig. 12. Normalized average error for Gain$_\theta$ in the *xz*-plane cut.

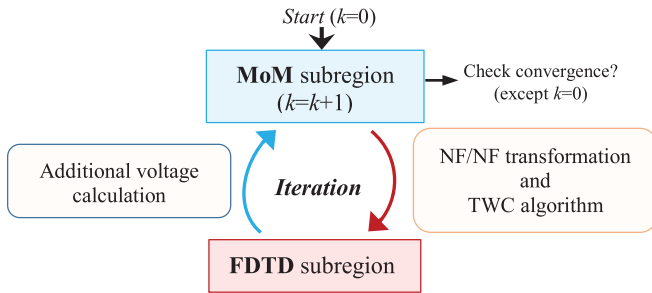Fig. 13. Geometrical representation of the MoM and FDTD subregions.



Fig. 14. Iterative procedure between MoM and FDTD subregion.

The procedure uses the MoM solution [27] for the electric current on the thin wire. This solution is

$$[\boldsymbol{I}_{\text{MoM}}(\omega_n)] = [Z(\omega_n)]^{-1} [V(\omega_n)], n = 0, 1, \ldots, N \quad (17)$$

$$[V(\omega_n)] = < \mathbf{E}^{\text{inc}}(\mathbf{r}, \omega_n), t(\mathbf{r} - \mathbf{r}_m) > \quad (18)$$

where $<>$ indicates the scalar product of the two enclosed vector functions of $\mathbf{r}$, $\mathbf{r}$ is the radius vector from the origin to a point on the antenna, $\omega_n$ is one of the angular frequencies of interest, $t(\mathbf{r} - \mathbf{r}_m)$ is the $m$th testing function, $\mathbf{r}_m$ is a specified point on the $m$th testing function, and $\mathbf{E}^{\text{inc}}(\mathbf{r}, \omega_n)$ is the incident electric field. In (17) and (18), $I_{MoM}$, $\mathbf{E}^{\text{inc}}$, and $V$ are actually the phasors of quantities that have $e^{j\omega_n t}$ dependence. If $M$ expansion functions are used, then $[Z(\omega_n)]$ is the $M \times M$ moment matrix and $[V(\omega_n)]$ and $[\boldsymbol{I}_{MoM}(\omega_n)]$ are $M \times 1$ matrices. The electric current on the antenna due to the incident electric field is a linear combination of the expansion functions where the $m$th element of $[\boldsymbol{I}_{MoM}(\omega_n)]$ in (17) multiplies the $m$th expansion function.

### A. Iterative Procedure for the Hybrid Problem

In the initialization, the antenna, driven by one volt across its input terminals, radiates in free space in the absence of the dielectric object. There is no incident field other than that which produces the one volt. Substitution of the impulsive electric field associated with the one volt into (18) gives $[V(\omega_n)] = V^0(\omega_n)$ which, when substituted into (17), gives $[\boldsymbol{I}_{MoM}(\omega_n)] = \boldsymbol{I}^0_{MoM}(\omega_n)$. In the following iterations, the one volt across the antenna input terminals is maintained by a zero impedance voltage source of one volt.

At the beginning of iteration $\#k$, using the near field formulation for the thin wire antenna [28] at all

frequencies of interest, the free space field of the electric current $I^{k-1}_{MoM}(\omega_n)e^{j\omega_n t}$ on the antenna is calculated for $(n = 1, 2, \ldots, N)$ on the TF/SF boundary in the FDTD subregion. Henceforth, this field will be called the incident field in the FDTD subregion. The incident field in the FDTD subregion is simulated by a TWC field similar to that in Section II-B2. The simulation of the incident field in the FDTD subregion starts an FDTD procedure that finds scattered electric and magnetic fields $\mathbf{e}^k_{\text{FDTD},s}(\mathbf{r}_{\text{IS}}, t)$ and $\mathbf{h}^k_{\text{FDTD},s}(\mathbf{r}_{\text{IS}}, t)$ on the IS in the FDTD subregion. Electric and magnetic currents $\mathbf{j}^k_{\text{FDTD}}(\mathbf{r}_{\text{IS}}, t) = \hat{n} \times \mathbf{h}^k_{\text{FDTD},s}(\mathbf{r}_{\text{IS}}, t)$ and $\mathbf{m}^k_{\text{FDTD}}(\mathbf{r}_{\text{IS}}, t) = -\hat{n} \times \mathbf{e}^k_{\text{FDTD},s}(\mathbf{r}_{\text{IS}}, t)$ and their Fourier transforms $\mathbf{J}^k_{\text{FDTD}}(\mathbf{r}_{\text{IS}}, \omega) = \hat{n} \times \mathbf{H}^k_{\text{FDTD},s}(\mathbf{r}_{\text{IS}}, \omega)$ and $\mathbf{M}^k_{\text{FDTD}}(\mathbf{r}_{\text{IS}}, \omega) = -\hat{n} \times \mathbf{E}^k_{\text{FDTD},s}(\mathbf{r}_{\text{IS}}, \omega)$ are defined at $\mathbf{r}_{\text{IS}}$ on the IS in the FDTD subregion where $\hat{n}$ is the outward directed unit vector that is perpendicular to the IS in the FDTD subregion. Next, for $(n = 1, 2, \cdots, N)$, $\mathbf{J}^k_{\text{FDTD}}(\mathbf{r}_{\text{IS}}, \omega_n)$ and $\mathbf{M}^k_{\text{FDTD}}(\mathbf{r}_{\text{IS}}, \omega_n)$ are calculated concurrently with $\mathbf{j}^k_{\text{FDTD}}(\mathbf{r}_{\text{IS}}, t)$ and $\mathbf{m}^k_{\text{FDTD}}(\mathbf{r}_{\text{IS}}, t)$ by means of the NFT [23] [see (8) and (9)]. Similar to the $e^{j\omega_n t}$ dependent parts of the electric and magnetic currents on the IS in subregion $d$ in Section II-B2, the $e^{j\omega_n t}$ dependent parts of the electric and magnetic currents on the IS in the FDTD subregion due to the incident field in the FDTD subregion are $\mathbf{J}^k_{\text{FDTD}}(\mathbf{r}_{\text{IS}}, \omega_n) e^{j\omega_n t}$ and $\mathbf{M}^k_{\text{FDTD}}(\mathbf{r}_{\text{IS}}, \omega_n) e^{j\omega_n t}$.

By the equivalence principle, the combination of the electric and magnetic currents $\mathbf{J}^k_{\text{FDTD}}(\mathbf{r}_{\text{IS}}, \omega_n) e^{j\omega_n t}$ and $\mathbf{M}^k_{\text{FDTD}}(\mathbf{r}_{\text{IS}}, \omega_n) e^{j\omega_n t}$ radiates its free space field beyond the IS in the FDTD subregion and no field in the region enclosed by the IS in the FDTD subregion. For $(n = 1, 2, \ldots, N)$, the phasor of the $e^{j\omega_n t}$ dependent part of this free space electric field, calculated on the surface of the antenna in the MoM subregion by using the NF/NF transformation [18], is substituted for $\mathbf{E}^{\text{inc}}(\mathbf{r}, \omega_n)$ in (18) to produce $[V(\omega_n)] = [V^k(\omega_n)]$ where $[V^k(\omega_n)]$ is the column matrix of phasors of incremental voltages. Substitution of $[V(\omega_n)] = [V^k(\omega_n)]$ into (17) gives $[\boldsymbol{I}_{MoM}(\omega_n)] = [\boldsymbol{I}^k_{MoM}(\omega_n)]$ where $[\boldsymbol{I}^k_{MoM}(\omega_n)]$ is the column matrix of phasors of incremental currents.

### B. Reckoning at Iteration $\# K$

The iteration procedure continues until a stopping criterion achieved. The stopping criterion is $\varepsilon_K$ where $K \geq 1$ indicates the $K$th iteration and $\varepsilon_K$ is given by

$$\varepsilon_K = \text{mean}_{n=1,2,\ldots,N} \left( \frac{\|\boldsymbol{I}^K_{MoM}(\omega_n)\|}{\|\sum_{k=0}^{K} \boldsymbol{I}^k_{MoM}(\omega_n)\|} \right) \times 100\% \quad (19)$$

where $\text{mean}_{n=1,2,\ldots,N}()$" indicates the average taken over $(n = 1, 2, \ldots, N)$ of the $n$-dependent quantity enclosed in the parentheses. Based on numerical experiments, it is sufficient to stop the iteration process at iteration $\#K$ in which $\varepsilon_K \leq 1\%$.

After completion of the $K$th iteration, the antenna impedance at $\omega = \omega_n$ is $Z^K(\omega_n)$ given by

$$Z^K(\omega_n) = \frac{1}{\sum_{k=0}^{K} \boldsymbol{I}_{in}\left([\boldsymbol{I}^k_{MoM}(\omega_n)]\right)} \quad (20)$$
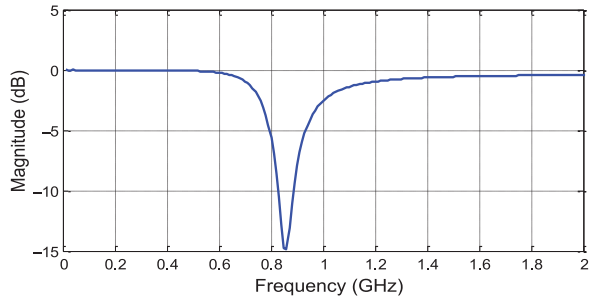
Fig. 15. Magnitude of the reflection coefficient of a single thin wire antenna.

TABLE I
ANTENNA INPUT IMPEDANCES AT FREQUENCIES OF INTEREST OF A
SINGLE THIN WIRE

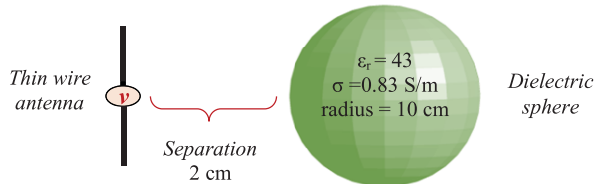| Method\freq. | 840 MHz | 860 MHz | 880 MHz |
|---|---|---|---|
| FDTD | 66.97 −j 21.19 | 72.14 +j 0.96 | 77.73 +j 23.17 |
| MoM | 67.63 −j 19.15 | 72.56 +j 3.03 | 77.82 +j 25.12 |



Fig. 16. Geometry of the problem.

where the numerator "1" represents the 1-V source across the antenna terminals. In the denominator, $I_{in}\left(\left[I_{MoM}^k(\omega_n)\right]\right)$ is the electric current determined at the input terminals of the antenna by the elements of $\left[I_{MoM}^k(\omega_n)\right]$.

### C. Results for Hybrid Problems

For the simulations presented here, a thin wire antenna with length of 16.65 cm and radius of 0.27 mm is used. The antenna input reflection coefficient is computed using the FDTD method in order to determine the frequency band in which it radiates well. The frequencies 840, 860, and 880 MHz are found to be in the band of operation. Fig. 15 shows the magnitude of the reflection coefficient of this antenna.

In the MoM simulation, piecewise sinusoids are chosen as expansion functions and point matching is used for testing. The tangential component of the electric field produced by a piecewise sinusoid is analytically given [29].

In order to show the difference between the results generated by MoM and FDTD methods, the input impedances of the thin wire antenna at frequencies of interest are shown in Table I.

In Fig. 16 which shows the geometry of the problem, the dielectric sphere placed a distance of 2 cm away from the thin wire antenna has a radius of 10 cm, relative permittivity of 43, and conductivity of 0.83 S/m. The thin wire antenna is divided into 51 segments for the MoM simulation and the discretization of the dielectric sphere is 2.5 mm in all Cartesian directions in FDTD simulations, leading to a total of 1.56 million cells used. Also, the entire problem space is solved using
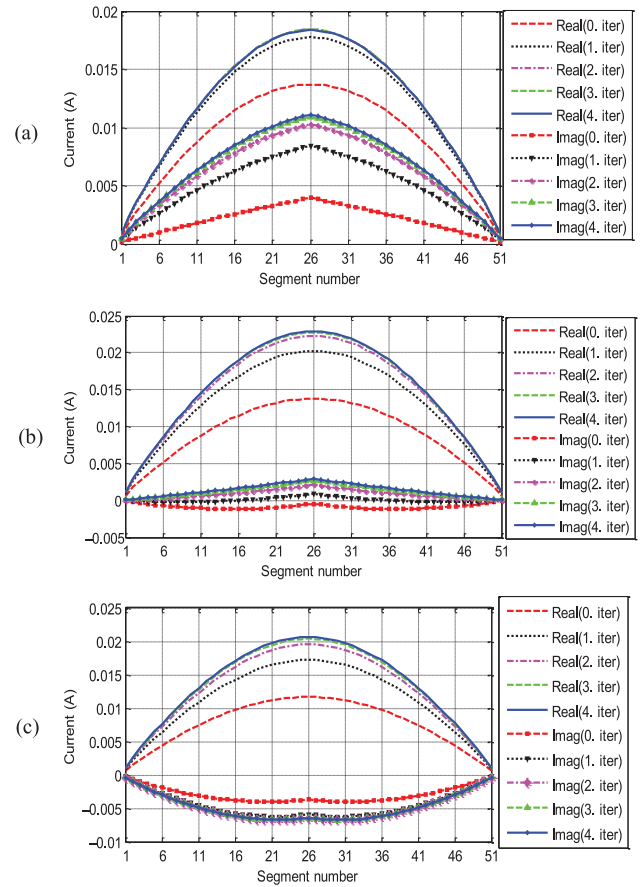


Fig. 17. Convergence of current distribution (real and imaginary part) versus segment number at frequencies: (a) 840, (b) 860, and (c) 880 MHz. Numbers (0–4) represent the iteration number.

TABLE II
ANTENNA INPUT IMPEDANCES AT FREQUENCIES OF INTEREST AFTER
FOUR ITERATIONS

| Method\freq. | 840 MHz | 860 MHz | 880 MHz |
|---|---|---|---|
| Full FDTD | 40.44 −j 28.58 | 43.15 −j 6.74 | 46.09 +j 15.21 |
| Hybrid | 40.15 −j 24.04 | 43.05 −j 5.29 | 44.00 +j 14.02 |

the FDTD method as a reference. For this full domain FDTD simulation, the discretization is 1.665 mm, which leads to a total of 4.4 million cells used. The computation time of the full domain simulation is 113 min, while that of the hybrid simulation after four iterations is 87 min. The current distributions over the antenna surface at 840, 860, and 880 MHz obtained using the hybrid method are shown in Fig. 17. The comparison of input impedances from the hybrid and the full FDTD methods is shown in Table II. This numerical comparison shows that the proposed hybrid results after four iterations are in good agreement with the conventional full domain FDTD method results.

A more complex configuration is presented in Fig. 18 to prove the validity of the proposed hybrid method for a problem which has multiple scattering objects close to the thin wire antenna. A conducting box and dielectric sphere are placed distances on the *x*-axis of 5 and 15 cm away from the thin wire
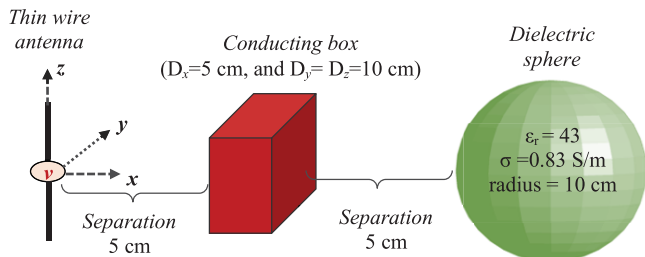
Fig. 18. Geometry of the problem.

TABLE III
ANTENNA INPUT IMPEDANCES AT FREQUENCIES OF INTEREST AFTER
EIGHT ITERATIONS

| Method\freq. | 840 MHz | 860 MHz | 880 MHz |
|---|---|---|---|
| Full FDTD | 25.01 –j 18.74 | 26.68 +j 7.51 | 29.11 +j 34.55 |
| Hybrid | 24.13 –j 20.10 | 25.87 +j 5.88 | 27.24 +j 33.67 |

antenna. The dimensions of the conducting box are 5 cm on the $x$-axis and 10 cm on the $y$- and $z$-axes. The dielectric sphere has a radius of 0.1 m, relative permittivity of 43, and conductivity of 0.83 S/m. The comparison of input impedances at 840, 860, and 880 MHz from the hybrid and the full FDTD methods is shown in Table III. This numerical comparison shows that the proposed hybrid results after eight iterations are in good agreement with the conventional full domain FDTD method results. The thin wire antenna is divided into 51 segments for the MoM simulation and the discretizations of the dielectric sphere and conducting box are 2.5 mm in all Cartesian directions in FDTD simulations, leading to a total of 1.88 million cells used. Also, the entire problem space is solved using the FDTD method as a reference. For this full domain FDTD simulation, the discretization is 1.665 mm, which leads to a total of 6.4 million cells used. The computation time of the full domain simulation is 176 min, while that of the hybrid simulation after eight iterations is 269 min. A considerable reduction in the memory storage requirements is achieved, but the computation time of the IMR algorithm is more than that of the full domain because of small separation between the objects. The computation time would be less and the memory reduction would be more for problems that have large separation between the objects and antenna.

## VI. CONCLUSION

In this paper, the integration of the FDTD method into the IMR technique is presented to obtain solutions at prespecified frequencies for large-scale electromagnetic scattering and radiation problems. Also, a hybrid method which combines the desirable features of two different numerical methods, MoM and FDTD, is presented to provide efficient and desirable solutions at multiple frequencies to antenna problems. The key contribution here is to construct a time-limited waveform which includes in its frequency spectrum the required magnitudes and phases of the time-harmonic signals of the desired solution frequencies. Furthermore, a remarkable saving in computer memory, and for some configurations a saving in the CPU time is achieved.

## REFERENCES

[1] B. Despres, "Domain decomposition method and the Helmholtz problem," in *Proc. Int. Symp. Math. Numer. Aspects Wave Propag. Phenom.*, Strasbourg, France, 1992, pp. 44–52.

[2] B. Stupfel and B. Despres, "A domain decomposition method for the solution of large electromagnetic scattering problems," *J. Electromagn. Waves Appl.*, vol. 13, no. 11, pp. 1553–1568, 1999.

[3] J. Wang and W. Hong, "A fast-domain decomposition method for electromagnetic scattering analysis of 3-D objects," in *Proc. Asia-Pac. Microw. Conf.*, 2000, pp. 424–427.

[4] Z. Qian, L. Yin, and W. Hong, "Application of domain decomposition and finite element method to electromagnetic compatible analysis," in *Proc. IEEE Antennas Propag. Soc. AP-S Int. Symp. Dig.*, 2001, vol. 4, pp. 642–645.

[5] P. Liu and Y.-Q. Jin, "The finite-element method with domain decomposition for electromagnetic bistatic scattering from the comprehensive model of a ship on and a target above a large-scale rough sea surface," *IEEE Trans. Geosci. Remote Sens.*, vol. 42, no. 5, pp. 950–956, May 2004.

[6] P. Paul and J. P. Webb, "Reducing computational costs using a multiregion finite element method for electromagnetic scattering," *IET Microw. Antennas Propag.*, vol. 2, no. 5, pp. 427–433, Aug. 2008.

[7] O. Ozgun and M. Kuzuoglu, "Iterative leap-field domain decomposition method: A domain decomposition finite element algorithm for 3D electromagnetic boundary value problems," *IET Microw. Antennas Propag.*, vol. 4, no. 4, pp. 543–552, Apr. 2010.

[8] A. Takei, S. Sugimoto, M. Ogino, S. Yoshimura, and H. Kanayama, "Full wave analyses of electromagnetic fields with an iterative domain decomposition method," *IEEE Trans. Magn.*, vol. 46, no. 8, pp. 2860–2863, Aug. 2010.

[9] M. H. Al Sharkawy, V. Demir, and A. Z. Elsherbeni, "Iterative Multi-Region Technique for large scale electromagnetic scattering problems—Two-dimensional case," *Radio Sci.*, vol. 40, no. 5, pp. 108–120, Sep. 2005.

[10] M. H. Al Sharkawy, V. Demir, and A. Z. Elsherbeni, "Scattering from two dimensional problems using the iterative multi-region technique for large scale problems based on the FDFD method," in *Proc. IEEE Antennas Propag. Soc. Int. Symp.*, Jul. 3–8, 2005, vol. 3B, pp. 188–191.

[11] M. H. Al Sharkawy, V. Demir, and A. Z. Elsherbeni, "The FDFD with the iterative multi-region technique for the scattering from multiple three dimensional objects," in *Proc. IEEE/ACES Int. Conf. Wireless Commun. Appl. Comput. Electromagn.*, Honolulu, HI, USA, 2005, pp. 732–735.

[12] M. H. Al Sharkawy, V. Demir, and A. Z. Elsherbeni, "Plane wave scattering from three dimensional multiple objects using the iterative multiregion technique based on the FDFD method," *IEEE Trans. Antennas Propag.*, vol. 54, no. 2, pp. 666–673, Feb. 2006.

[13] G. Zheng and B.-Z. Wang, "Analysis of scattering from multiple objects by the finite-difference frequency-domain method with an iteration-free multiregion technique," *IEEE Antennas Wireless Propag. Lett.*, vol. 8, 794–797, Jul. 2009.

[14] M. Carr and J. L. Volakis, "Domain decomposition by iterative field bouncing," in *Proc. IEEE Antennas Propag. Soc. AP-S Int. Symp. (Dig.)*, San Antonio, TX, USA, 2002, vol. 3, pp. 298–301.

[15] F. Xu and W. Hong, "Analysis of two dimensions sparse multicylinder scattering problem using DD-FDTD method," *IEEE Trans. Antennas Propag.*, vol. 52, no. 10, pp. 2612–2616, Oct. 2004.

[16] L. Yin, X. Yin, and W. Hong, "A fast algorithm based on DDM and FMM for scattering by multi-cylinders," in *Proc. Int. Symp. Antennas Propag. EM Theory (ISAPE)*, Beijing, China, 2000, pp. 195–198.

[17] J. M. Johnson and Y. Rahmat-Samii, "Multiple region FDTD (MR/FDTD) and its application to microwave analysis and modeling," in *Proc. IEEE MTT-S Int. Microw. Symp. Dig.*, San Francisco, CA, USA, 1996, pp. 1475–1478.

[18] C. A. Balanis, *Advanced Engineering Electromagnetics*. Hoboken, NJ, USA: Wiley, 1989.

[19] G. Cerri, P. Russo, A. Schiavoni, G. Tribellini, and P. Bielli, "MoM–FDTD hybrid technique for analyzing scattering problems," *Electron. Lett.*, vol. 34, pp. 438–440, 1998.

[20] M. A. Mangoud, R. A. Abd-Alhameed, and P. S. Excell, "Simulation of human interaction with mobile telephones using hybrid techniques over coupled domains," *IEEE Trans. Microw. Theory Techn.*, vol. 48, no. 11, pp. 2014–2021, Nov. 2000.

[21] S. Mochizuki, S. Watanabe, M. Taki, Y. Yamanaka, and H. Shirai, "Novel iteration procedures of a hybrid method combining MoM and scattered-field FDTD method for electromagnetic dosimetry," *Proc. IEEE Top. Conf. Wireless Commun. Technol.*, Honolulu, HI, USA, Oct. 2003, pp. 200–201.

[22] D. Wei, Z. Peiyun, Z. Yu, and L. Changhong, "Study on human head/antenna interactions with a novel hybrid MoM-FDTD method," in *Proc. Asia-Pac. Microw. Conf. (APMC)*, Dec. 4–7, 2005, vol. 3, pp. 174–178.

[23] A. Z. Elsherbeni and V. Demir, *The Finite-Difference Time-Domain Method for Electromagnetics With MATLAB Simulations*. Raleigh, NC, USA: SciTech, 2009.

[24] A. Taflove and S. C. Hagness, *Computational Electrodynamics: The Finite-Difference Time-Domain Method*, 2nd ed. Norwood, MA, USA: Artech House, 2000.

[25] J. A. Roden and S. D. Gedney, "Convolution PML (CPML): An efficient FDTD implementation of the CFS-PML for arbitrary media," *Microw. Opt. Technol. Lett.*, vol. 27, no. 5, pp. 334–339, 2000.

[26] J. L. Volakis, A. Chatterjee, and L. C. Kempel, *Finite Element Method for Electromagnetics: Antennas, Microwave Circuits, and Scattering Applications*. Hoboken, NJ, USA: Wiley-IEEE Press, 1998.

[27] R. F. Harrington, *Field Computation by Moment Methods*. New York, NY, USA: Macmillan, 1968 (reprinted by IEEE press), 1993.

[28] C. A. Balanis, *Antenna Theory: Analysis and Design*, 3rd ed. Hoboken, NJ, USA: Wiley, 2005.

[29] E. C. Jordan and K. G. Balmain, *Electromagnetic Waves and Radiating Systems*, 2nd ed. Englewood Cliffs, NJ, USA: Prentice-Hall, 1968.

**Fatih Kaburcuk** was born in Sivas, Turkey, in 1984. He received the B.Sc. degree from Ondokuz Mayis University, Samsun, Turkey, in 2007, and the M.Sc. and Ph.D. degrees from Syracuse University, Syracuse, NY, USA, in 2011 and 2014, respectively, all in electrical engineering.

He worked as a Research Assistant with PPC-Belden, Inc., Syracuse, NY, USA, in 2013. He worked as a Visiting Research Scholar at the Department of Electrical Engineering and Computer Science, Colorado School of Mines, Golden, CO, USA, in 2014. He has been serving as an Assistant Professor with the Department of Electrical and Electronics Engineering, Erzurum Technical University, Erzurum, Turkey. His research interests include electromagnetic scattering and microwaves.

**Veysel Demir** (M'05) received the Bachelor of Science degree from Middle East Technical University, Ankara, Turkey, in 1997, and the Master of Science and Doctor of Philosophy degrees from Syracuse University, Syracuse, NY, USA, in 2002 and 2004, respectively, all in electrical engineering.

He is an Associate Professor with the Department of Electrical Engineering, Northern Illinois University, DeKalb, IL, USA. During his graduate studies, he worked as a Research Assistant with Sonnet Software, Inc., Liverpool, NY, USA. He worked as a Visiting Research Scholar at the Department of Electrical Engineering, University of Mississippi, Oxford, MS, USA, from 2004 to 2007. He joined the Northern Illinois University in August 2007 and served as an Assistant Professor until August 2014. He has been serving as an Associate Professor since then.

Dr. Demir is a member of ACES and SigmaXi. He served as a Technical Program Co-Chair for the 2014 IEEE International Symposium on Antennas and Propagation and USNC-URSI Radio Science Meeting and for the ACES 2015 conference.

**Atef Z. Elsherbeni** (F'07) received the Ph.D. degree in electrical engineering from Manitoba University, Winnipeg, MB, Canada, in 1987.

He was with the University of Mississippi, Oxford, MS, USA, from 1987 to 2013. He was a Finland Distinguished Professor from 2009 to 2011. In August 2013, he became the Dobelman Distinguished Chair Professor of Electrical Engineering with Colorado School of Mines, Golden, CO, USA. He is currently the Interim Department Head of the Department of Electrical and Computer Science. His research interests include the scattering and diffraction of EM waves, finite-difference time-domain analysis of antennas and microwave devices, field visualization and software development for EM education, interactions of electromagnetic waves with the human body, RFID and sensor integrated FRID systems, reflector and printed antennas and antenna arrays, and measurement of antenna characteristics and material properties.

Dr. Elsherbeni is a Fellow of ACES. He is the Editor-in-Chief for *ACES Journal*. He was the General Chair for the 2014 APS-URSI Symposium and was the President of ACES Society from 2013 to 2015.

**Ercument Arvas** (F'03) was born in 1953, in Van, Turkey. He received the B.Sc. and M.Sc. degrees from Middle East Technical University, Ankara, Turkey, in 1976 and 1979, respectively, and the Ph.D. degree from Syracuse University, Syracuse, NY, USA, in 1983, all in electrical engineering.

From 1983 to 1984, he was with the Department of Electrical Engineering, Yildiz Technical University, Istanbul, Turkey. From 1984 to 1987, he was with Rochester Institute of Technology, Rochester, NY, USA, and from 1987 to 2014, he was with Syracuse University, Syracuse. He is currently teaching at the Department of Electronics Engineering, Istanbul Medipol University, Istanbul, Turkey. His research interests include electromagnetics scattering and microwave devices.

Dr. Arvas is a member of ACES and a Fellow of the Electromagnetics Academy.

**Joseph R. Mautz** (S'66–M'67–SM'75–F'05–LF'05) was born in Syracuse, NY, in 1939. He received the B.S., M.S., and Ph.D. degrees in electrical engineering from Syracuse University, Syracuse, NY, in 1961, 1965, and 1969, respectively.

Until July 1993, he was a Research Associate in the Electrical Engineering and Computer Science Department of Syracuse University where he worked on electromagnetic radiation and scattering problems. From August 1993 to August 2015, he had an office at Syracuse University, helping to advise many Ph.D. students. His research interest includes electromagnetic theory and applied mathematics.